ACS OMEGA

Open Access

http://pubs.acs.org/journal/acsodf

Article

Effects of Mechanical Properties on Gas−Water Flow Characteristics around Boreholes: Implementation of Damage-Based Coupling Models

Chunshan Zheng,* Haifei Wu, Guofu Li,* Sheng Xue, Bingyou Jiang, and Mingyun Tang

Cite This: *ACS Omega* 2024, 9, 19578−19590

Read Online

ACCESS | Metrics & More | Article Recommendations

ABSTRACT: Neglecting the coal damage effect around a borehole could result in low accuracy of gas extraction seepage analysis. A fluid−solid coupling model incorporating coal stress and damage, gas diffusion, and seepage was established. Reliability of the proposed model was validated using field data. Variation characteristics of gas−water phase parameters in the borehole damage zone during gas drainage were analyzed. Meanwhile, effects of equivalent plastic strain, lateral pressure coefficient, internal friction angle, cohesion, Young's modulus, and Poisson's ratio on the damage state and spatiotemporal change properties of gas extraction flow were investigated. Results indicate that due to coal damage, permeability shows a three-zone distribution around the borehole, among which the fracture zone has the highest permeability, approximately 40 times of the original value. Permeability in the plastic zone decreases rapidly, while permeability is the smallest in the elastic zone. Coal permeability within the damage zone increases with continuous gas extraction. A smooth and low-value zone occurs for both fracture and matrix gas pressures. With the increase in equivalent plastic strain, the damage zone decreases, while peak permeability in the damage zone rises, and gas pressure in the smooth low-pressure zone continues to drop. The damage zone becomes smaller with an increasing lateral pressure coefficient, while those plastic and elastic zones become larger. The damage zone area corresponding to the lateral pressure coefficient of 0.89 is 82.3% smaller compared with that of 0.56. As internal friction angle and cohesion rise, the damage zone gradually decreases and shifts from a butterfly shape to elliptical shape. When Young's modulus is heterogeneously distributed, except for concentrated shear damage zones around the borehole, punctate microdamage zones are also found at positions far from the borehole. Those damage zones gradually become smaller as shape parameters of the Weibull distribution get larger. The above findings are expected to offer theoretical support and practical guidance for borehole drilling and efficient extraction of clean methane resources.

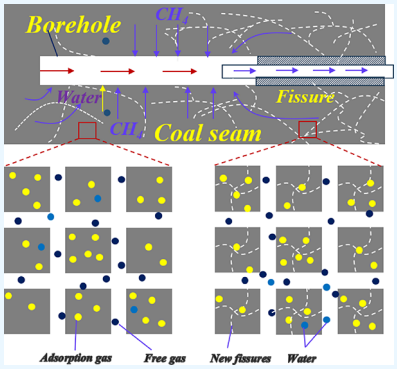

1. INTRODUCTION

Methane predrainage could help preventing coal and gas outbursts. Drilling gas extraction boreholes into coal seam forms channels for gas flow and relieves stress around the borehole.[1,2] However, many CBM reservoirs are characterized by high gas contents, low permeability, and strong heterogeneity.[3−5] To improve the gas extraction effect, borehole enlarging methods, such as hydraulic slotting and hydraulic flushing, are often adopted in low-permeability coal seams, thus achieving permeability enhancement.[6,7] It should be pointed out that borehole drilling and enlarging methods often cause damage, forming different ranges of fractured zones or collapsed zones around the borehole. This damage effect significantly affects geological engineering projects and gas extraction design as permeability could rise by hundreds of times in damaged coal.[8,9]

Some research studies on borehole gas extraction have been conducted.[10] Fan and Ettehadtavakkol[11] analyzed transport of fluids in shale gas reservoirs around multistage fractured horizontal wells and established a multistage fluid transport multifield coupling model based on differences in transport mechanism for analyzing relative contributions of fluid transport at different stages to gas production. Zhang et al.[12] used gas extraction experimental systems to explore effects of superposed impacts of borehole groups on gas extraction. Zhang et al.[13] studied permeability distribution around boreholes after hydraulic flushing through theoretical analysis and numerical simulation. Cao et al.[14] studied gas and water phase flow patterns around boreholes based on their multiscale multiphase simulation model. Chen et al.[15] established an anisotropic permeability model and quantitatively analyzed gas transport

Received: February 7, 2024
Revised: March 30, 2024
Accepted: April 3, 2024
Published: April 16, 2024

patterns under different permeability anisotropy ratios. Duan et al.[16] established a dynamic permeability anisotropy model and explored the effect of anisotropy ratio on gas pressure distribution. Fang et al.[17] established a multifield coupling model and studied gas pressure distribution as well as effective extraction radius of boreholes. Liu et al.[18] explored gas seepage and diffusion characteristics in coal based on an improved permeability model. Through adopting an established coupling model, Zheng et al.[19] revealed that the permeability of damaged coal under a goaf area increased by more than 650 times. Qi et al.[20] explored the influence of temperature field on gas fracturing technology based on an established thermal−fluid−solid coupling model.

However, most of the previous related studies considered coal seam homogeneity, particularly neglecting the impact of coal damage on gas extraction seepage properties. Neglecting the effect of coal damage on permeability could significantly underestimate the permeability value around the borehole during gas extraction processes. As shown in Figure 1, fractured

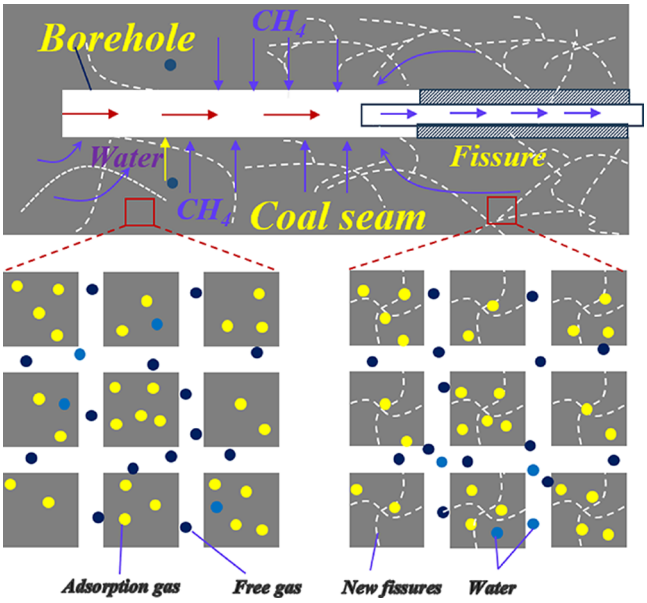

Figure 1. Conceptual model of damage around gas drainage boreholes.

zones are formed around boreholes. New fractures tend to be randomly distributed, which increases coal permeability.[21,22] This phenomenon has been proved in the permeability experiment of Wang et al.,[23] i.e., permeability shows a sharp upward trend in damaged coal. In view of the above issue, this study develops a coupled gas seepage model considering damage around the borehole. Meanwhile, a Weibull distribution is introduced to realize coal heterogeneity. Gas and water phase flow properties in the borehole damaged zone are analyzed. Results could help to reasonably assess the damage condition around the borehole and its effect on the gas extraction process as well as provide theoretical guidance for efficient borehole sealing.

2. MATHEMATICAL MODEL

Based on the following assumptions, a multifield coupled model comprehensively considering coal stress, gas seepage, gas diffusion, and coal damage is established in this study, aiming to accurately analyze the impact of borehole-drilling-induced damage on gas extraction flow patterns.[24−26]

(1) Coal is assumed to have microscopic and macroscopic pores intertwined with each other.
(2) Gas flow in the matrix and cracks follows Fick's law and Darcy's law, respectively.
(3) Water exists only in the crack system, and its flow follows generalized Darcy's law.
(4) Impacts of the coal seam temperature are ignored. Gas adsorption follows the Langmuir adsorption equilibrium equation.

2.1. Coal Deformation Control Equation and Damage Criterion. Coal is assumed to have a pore-fracture structure. With comprehensively considering the effects of ground stress, gas pressure, gas adsorption and desorption, and volumetric stress on coal seam after borehole drilling, the coal stress equation could be expressed as follows[27,28]:

$$\varepsilon_{ij} = \frac{1}{2G}\sigma_{ij} - \left(\frac{1}{6G} - \frac{1}{9K}\right)\sigma_{kk}\delta_{ij} + \frac{\alpha_m p_m \delta_{ij} + \alpha_f p_f \delta_{ij}}{3K} + \frac{\varepsilon_s \delta_{ij}}{3} \quad (1)$$

where K is the bulk modulus of coal, $K = E/3(1-2\upsilon)$; K_m is bulk modulus of the coal matrix, $K_m = E_m/3(1-2\upsilon)$; K_s is the bulk modulus of the coal skeleton; E is the elastic modulus of coal (MPa), while E_m is the elastic modulus of the coal matrix; ε_{ij} is the strain tensor; σ_{ij} is the total stress; $\alpha_f = (1-K)/K_m$ represents the effective stress coefficient in fracture, while $\alpha_m = K/K_m - K/K_s$ denotes the effective stress coefficient in the matrix; δ_{ij} denotes the Kronecker symbol.

Taking into account the continuity of coal deformation, the stress equilibrium equation and geometric equation of coal could be expressed as[29]

$$\begin{cases} \sigma_{ij,j} + f_i = 0 \\ \varepsilon_{ij} = \frac{1}{2}(u_{i,j} + u_{j,i}) \end{cases} \quad (2)$$

Ignoring the impact of coal temperature, volume strain ε_s generated by coal adsorption follows the Langmuir curve:

$$\varepsilon_s = \varepsilon_L \frac{p_m}{p_m + p_L} \quad (3)$$

Based on eqs 1, 2, and 3, the coal deformation control equation could be derived as follows[30]:

$$Gu_{i,jj} + \frac{G}{1-2\nu}u_{j,ji} - \alpha_m p_{m,i} - \alpha_f p_{f,i} - K\varepsilon_{s,i} + F_i = 0 \quad (4)$$

Drilling boreholes in gas-containing coal seam causes stress and cracks around the borehole to redistribute, forming a fractured zone, a plastic zone, and an elastic zone. In terms of the damage criterion for gas-containing coal, DP criterion is selected in this study[31]:

$$F = \sqrt{J_2} + \alpha I_1 - k \quad (5)$$

where I_1 is the first invariant of stress tensor and J_2 is the second invariant of stress bias.

DP criterion matches the Mohr−Coulomb criterion under planar strain conditions. Relevant parameters are as follows:

$$\alpha = \frac{\tan\phi}{\sqrt{9 + 12\tan^2\phi}} \quad (6)$$

https://doi.org/10.1021/acsomega.4c01081
ACS Omega 2024, 9, 19578−19590

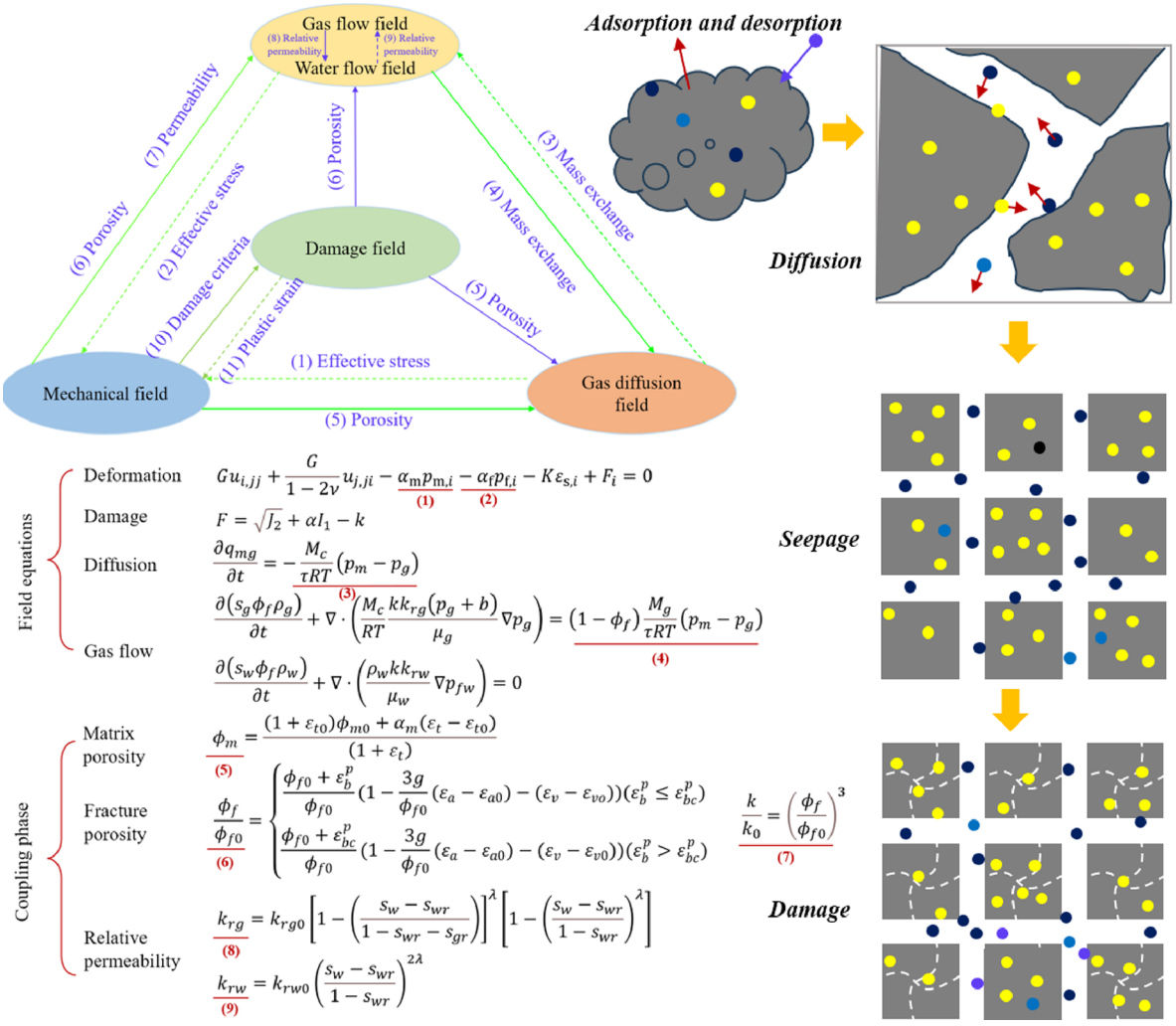

Figure 2. Schematic diagram of multifield coupling relationship.

$$k = \frac{3c}{\sqrt{9 + 12\tan^2\phi}} \tag{7}$$

where c represents the cohesion and ϕ indicates the internal friction angle.

2.2. Gas−Water Phase Seepage Field. Gas and water in deep coal seams are in a dynamic equilibrium. However, borehole gas extraction disturbs this equilibrium. According to the law of conservation of mass, transport of gas and water in coal seams follows the generalized Darcy's law, namely[32]:

$$\begin{cases} \dfrac{\partial q_{fg}}{\partial t} = -\nabla\cdot(\rho_g v_g) + (1-\phi_f)Q_m \\ \dfrac{\partial q_{fw}}{\partial t} = -\nabla\cdot(\rho_w v_w) \end{cases} \tag{8}$$

where ρ_g and ρ_w represent the densities of gas and water, respectively (kg/m^3); ϕ_f represents the coal fracture porosity; Q_m represents the mass source exchanged between the matrix and fracture system. q_{fg} and q_{fw} represent the mass of gas and water in cracks, respectively, which could be defined as follows:

$$\begin{cases} q_{fg} = s_g\phi_f\rho_g \\ q_{fw} = s_w\phi_f\rho_w \end{cases} \tag{9}$$

The flow rate of gas and water in coal is

$$\begin{cases} v_g = -\dfrac{kk_{rg}}{\mu_g\left(1+\frac{b}{p_g}\right)}\nabla p_g \\ v_w = -\dfrac{kk_{rw}}{\mu_w}\nabla p_{fw} \end{cases} \tag{10}$$

where v_g and v_w represent the gas and water flow rates in coal seam derived from Darcy's law (m/s), μ_g and μ_w represent the dynamic viscosities of gas and water, respectively (Pa·s), while b represents the Klinkenberg factor.

The law of conservation of mass and Darcy's law are commonly used to describe the movement characteristics for each component in a multiphase flow. Coal cracks usually contain two fluids: gas and water. Their seepage properties depend on the relative permeability and effective saturation. k_{rg} and k_{rw} represent the relative permeabilities of gas and water, respectively (m^2), which could be expressed as[2]

https://doi.org/10.1021/acsomega.4c01081
ACS Omega 2024, 9, 19578−19590

$$\begin{cases} k_{rg} = k_{rg0}\left[1 - \left(\dfrac{s_w - s_{wr}}{1 - s_{wr} - s_{gr}}\right)\right]^{\lambda}\left[1 - \left(\dfrac{s_w - s_{wr}}{1 - s_{wr}}\right)^{\lambda}\right] \\ k_{rw} = k_{rw0}\left(\dfrac{s_w - s_{wr}}{1 - s_{wr}}\right)^{2\lambda} \end{cases} \tag{11}$$

where s_w is the water saturation and s_g is the gas saturation. s_w and s_g have the following relationship:

$$s_g + s_w = 1 \tag{12}$$

By combining eqs 8, 9, 10, 11, and 12, the flow of gas and water could be expressed as

$$\begin{cases} \dfrac{\partial(s_g\phi_f\rho_g)}{\partial t} + \nabla\cdot\left(\dfrac{M_c}{RT}\dfrac{kk_{rg}(p_g + b)}{\mu_g}\nabla p_g\right) \\ \quad = (1 - \phi_f)\dfrac{M_g}{\tau RT}(p_m - p_g) \\ \dfrac{\partial(s_w\phi_f\rho_w)}{\partial t} + \nabla\cdot\left(\dfrac{\rho_w kk_{rw}}{\mu_w}\nabla p_{fw}\right) = 0 \end{cases} \tag{13}$$

2.3. Gas Diffusion Field. The gas transport process in a coal matrix is driven by a concentration gradient and mainly in the form of Fick diffusion. At any given moment, the amount of adsorbed gas and free gas in pores equals the amount of gas diffusing into fractures. This indicates that the total amount of gas in coal remains unchanged, with dynamic exchanges between adsorbed gas and free-form gas. Gas exchange between the matrix and fractures follows the following equation[33]:

$$Q_m = D_t\tau(c_m - \rho_f) \tag{14}$$

Gas in the coal matrix includes adsorbed and free gas[26]:

$$q_{mg} = \frac{abp_m\rho_c M_C}{(1 + bp_m)V_m} + \phi_m\frac{M_C p_m}{RT} \tag{15}$$

Due to the complex and variable geometry of the coal matrix, it is difficult to directly determine the gas diffusion rate in it. Therefore, adsorption time is usually used to represent the matrix gas diffusion rate:

$$\tau = \frac{1}{\sigma_c D} \tag{16}$$

where D denotes the gas diffusion coefficient ($m^2\cdot s^{-1}$) and σ_c represents the coal matrix's shape factor ($\sigma_c = 3\pi^2/L^2$).

According to Fick's law of diffusion, the gas transport equation in the coal matrix is[34,35]

$$\frac{\partial q_{mg}}{\partial t} = -\frac{M_c}{\tau RT}(p_m - p_g) \tag{17}$$

2.4. Coupling Models. Coal matrix pores serve as the main gas storage space, and their change is a complex process affected by a variety of factors. Specifically, coal matrix evolution is jointly determined by coal volume change, matrix gas pressure, and gas adsorption. Evolution of coal matrix porosity can be expressed as[36]

$$\phi_m = \frac{(1 + \varepsilon_{t0})\phi_{m0} + \alpha_m(\varepsilon_t - \varepsilon_{t0})}{(1 + \varepsilon_t)} \tag{18}$$

Considering that the matrix width at the time of damage is[37]

$$L_m = \frac{1}{n_{matrix} + 1}L_{m0} = \frac{\phi_{f0}}{\varepsilon_b^P + \phi_{f0}}L_{m0} \tag{19}$$

Fracture porosity is

$$\frac{\phi_f}{\phi_{f0}} = \frac{L_f}{L_{f0}}\cdot\frac{L_{m0}}{L_m} \tag{20}$$

Assuming coal porosity remaining unchanged during the residual stage, fracture porosity can be as follows based on eqs 19 and 20:

$$\frac{\phi_f}{\phi_{f0}} = \left(1 + \frac{\Delta L_f}{L_f}\right)\cdot\frac{L_{m0}}{L_m} = \begin{cases} \dfrac{\phi_{f0} + \varepsilon_b^P}{\varphi_{f0}}(1 + \Delta\varepsilon_f) & (\varepsilon_b^P \le \varepsilon_{bc}^P) \\ \dfrac{\phi_{f0} + \varepsilon_{bc}^P}{\varphi_{f0}}(1 + \Delta\varepsilon_f) & (\varepsilon_b^P > \varepsilon_{bc}^P) \end{cases} \tag{21}$$

where ε_{bc}^P characterizes the degree of damage around the borehole, with $\varepsilon_{bc}^P = 0$ indicating coal permeability in the elastic stage and $\varepsilon_{bc}^P \neq 0$ indicating permeability in the damage state.

In general, the cubic law exists between permeability and porosity:

$$\frac{k}{k_0} = \left(\frac{\phi_f}{\phi_{f0}}\right)^3 = \begin{cases} \left[\dfrac{\phi_{f0} + \varepsilon_b^P}{\phi_{f0}}\left(1 - \dfrac{3g}{\phi_{f0}}(\varepsilon_a - \varepsilon_{a0}) - (\varepsilon_v - \varepsilon_{v0})\right)\right]^3 \\ \quad (\varepsilon_b^P \le \varepsilon_{bc}^P) \\ \left[\dfrac{\phi_{f0} + \varepsilon_{bc}^P}{\phi_{f0}}\left(1 - \dfrac{3g}{\phi_{f0}}(\varepsilon_a - \varepsilon_{a0}) - (\varepsilon_v - \varepsilon_{v0})\right)\right]^3 \\ \quad (\varepsilon_b^P > \varepsilon_{bc}^P) \end{cases} \tag{22}$$

Figure 2 shows the aforementioned multifield coupling relationship, which is solved by adopting the PDE module of COMSOL Multiphysics software to analyze damage properties around boreholes and multiphase flow characteristics.

3. NUMERICAL MODELING

To investigate the gas extraction flow characteristics affected by borehole damage, a numerical model is developed based on parameters of the experimental mine (Figure 3). The modeling area has 40 m length and 4 m height. An overburden pressure of 18 MPa is applied to model the top, while the bottom side is set as the fixed constraint boundary. The left side is the roller boundary. The right side is constrained by a horizontal stress of 10 MPa. The borehole diameter is 100 mm. A monitoring line with a length of 3 m is set in the model. The monitoring point is 1 m to the right of the borehole. The left side is the gas extraction

https://doi.org/10.1021/acsomega.4c01081
ACS Omega 2024, 9, 19578−19590

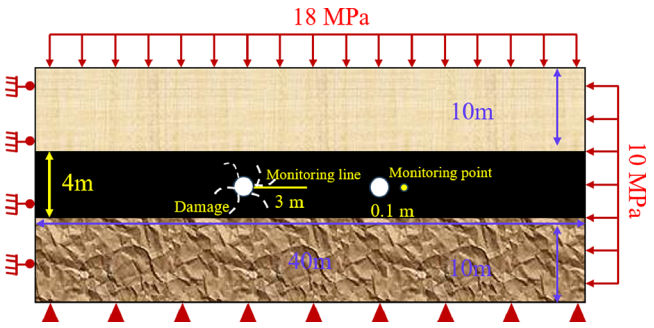

Figure 3. Schematic diagram of the numerical model.

borehole in the damaged area. The right side is the gas extraction borehole in elastic coal. Table 1 lists the numerical model parameters. These physical parameters are mainly obtained from field tests, physical experiments, and published references.

Table 1. Numerical Model Parameters

parameter	value	source
initial gas pressure p_0(MPa)	1.2	field data
Young's modulus E (MPa)	2500	experiments
original porosity	0.06	38
initial crack rate	0.01	39
water density ρ_w (kg/m^3)	1000	4
coal density ρ_c (kg/m^3)	1250	experiments
Poisson ratio ν	0.3	field data
cohesion C_0 (MPa)	2.5	field data
initial water saturation S_{w0}	0.6	experiments
plastic strain in residual phase ε_{bc}^{P}	0.02	36
gas adsorption time τ (day)	9.2	experiments
Langmuir pressure constant P_L (MPa)	1	experiments
Langmuir volume constant V_L (m^3/t)	20	experiments
geothermal temperature T (K)	293	field data
angle of internal friction φ_0 (deg)	20	36
initial permeability (mD)	0.01	experiments

4. RESULT ANALYSIS AND DISCUSSION

4.1. Gas Extraction Characteristics in Damaged Coal.

4.1.1. Model Validation. Seepage experiments are performed to validate the derived permeability model. Figure 4a shows that during the elastic stage, permeability gradually drops with increased confining pressure. Predictions of the permeability model fit well with laboratory data (R^2 = 0.90), including permeability values of damaged coal. Meanwhile, to verify accuracy of the theorectical model, gas extraction flow data of boreholes with good construction quality are collected. As shown in Figure 4b, coal seam water is rapidly drained in the early stage of gas extraction, while the gas flow rate shows a rapid downward trend after about 10 days. A comparison between simulated gas flow data and on-site data suggested that coal permeability model considering damage could well predict the fluctuation of field flow data.

4.1.2. Variation Characteristics of Gas−Water-Phase Parameters during Gas Extraction. Figure 5 shows the gas and water flow field distributions near the borehole at different extraction times. During gas extraction, gas and water pressures are different inside the coal. It could be observed that the gas pressure in the matrix and fracture and water phase pressure both show varying degrees of decline. In addition, the range of

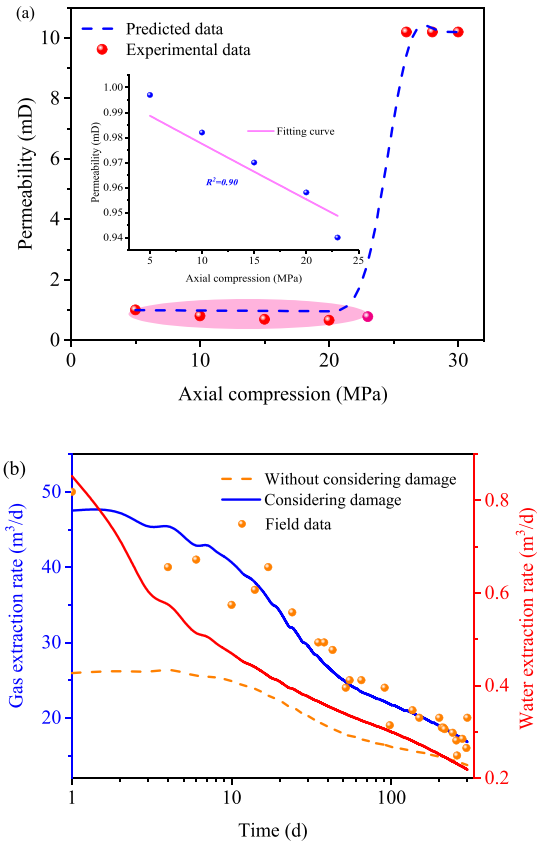

Figure 4. Matching analysis between theoretical model data and test data. (a) Permeability data; (b) extraction rate data.

the formed low-pressure zone gradually expands, indicating a wider low-pressure zone in coal. The matrix and fracture gas pressures near the borehole decrease from 1.2 to 0.02 MPa, while the water phase pressure drops from 1.06 to 0.02 MPa. The reason is a small fractured zone being formed near the borehole, resulting in a greater permeability, a lower gas and water flow resistance, and lower pressures of two phases.

Figure 6a shows the spatiotemporal variations of permeability. Spatially, a damage zone, a plastic zone, and an elastic zone are formed around the borehole. The damage zone has the biggest permeability, about 40 times the original permeability. Permeability in the plastic zone decreases rapidly, while permeability in the elastic zone is the smallest, gradually decreasing to the original value. Temporally, the permeability of the damage zone shows big changes with continuous gas extraction. In the initial stage, it increases rapidly, mainly due to gradual expansion of cracks and pores during gas extraction. However, the flow channels gradually stabilize. As a result, permeability growth gradually slows, which eventually tends to a relatively stable state. At drainage times of 1, 10, 100, and 300 days, the maximum permeability values are 34 k_0, 39 k_0, 45 k_0, and 46 k_0, respectively. However, it should be noted that the permeability in the elastic zone still increases significantly with extraction. As shown in Figure 6b, gas pressure in the coal matrix is always higher than that in fractures, which gradually decreases as extraction time becoming longer. A high-permeability zone is formed near the borehole due to fractured state, and fracture and matrix gas pressures form a smooth, low-value zone. In Figure 6c,d, the relative permeability of water is larger in the initial stage of gas drainage, while gas relative permeability gradually increases with continuous extraction. Finally, the gas pressure

https://doi.org/10.1021/acsomega.4c01081
ACS Omega 2024, 9, 19578−19590

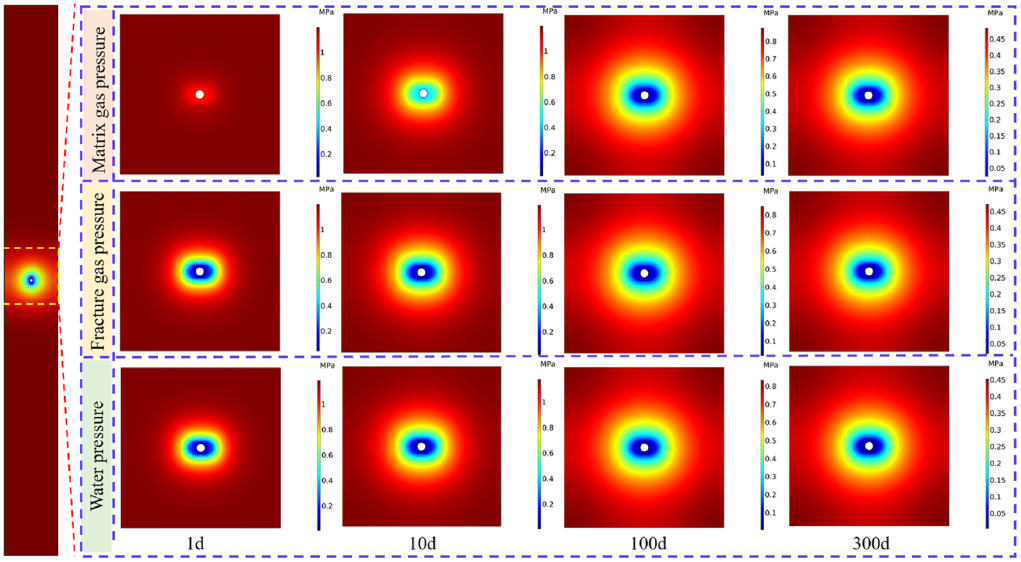

Figure 5. Gas and water phase pressures.

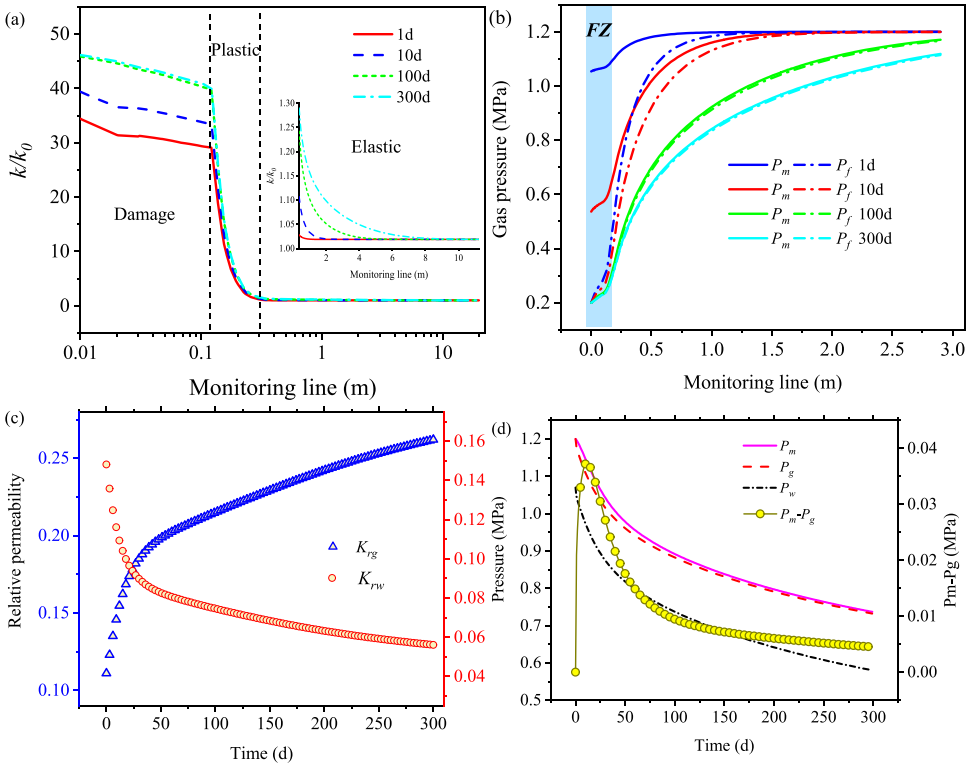

Figure 6. Gas extraction flow properties. (a) Permeability; (b) spatial evolution of gas pressure; (c) temporal evolution of gas and water pressures; (d) relative permeability of gas and water phases.

exceeds the water pressure. Hence, high water contents are not conducive to the early stage gas extraction.

Permeability and gas pressure distributions around the borehole are predicted using different theoretical models. Overall, permeability demonstrates a rising trend in the damage zone and plastic zone but remains basically unchanged in the elastic zone, as shown in Figure 7a. However, Liu et al.[18] and Su et al.[40] believe that the stress concentration around the borehole forms a permeability reduction zone, as shown in Figure 7b. In those two cases, permeabilities around the borehole considering and not considering damage are different, resulting in two different gas pressure spatial distributions in Figure 7c,d. Meanwhile, unlike the gas pressure distribution in Figure 7d, a smooth low gas pressure zone is formed around the borehole when considering the damage effect (Figure 7c). This phenomenon is more in line with the actual extraction process, which has been confirmed by various scholars.[6,41,42]

4.2. Sensitivity Analysis on Damage-Based Permeability and Gas Extraction Flow. *4.2.1. Effect of Equivalent Plastic Strain.* Drilling boreholes causes stress redistribution in coal, forming a fracture zone where coal permeability is significantly enhanced, providing gas transport channels. This section focuses on the effect of different equivalent plastic strains

https://doi.org/10.1021/acsomega.4c01081
ACS Omega 2024, 9, 19578−19590

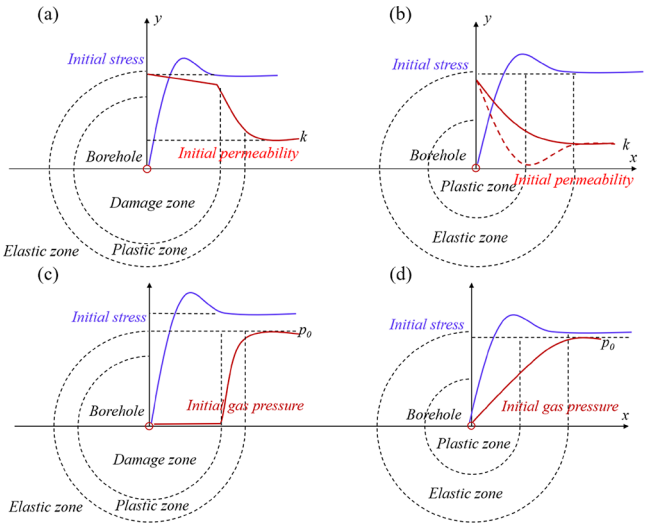

Figure 7. Comparison of permeability and pressure predictions by different theoretical models. (a) Permeability predicted by the damage-based model of this study; (b) permeability predicted by models of Liu et al.[18] and Su et al.[40]; (c) gas pressure corresponding to the damage-based model of this study; (d) gas pressure corresponding to models of Liu et al.[18] and Su et al.[40]

(ε_{bc}^{P}) on coal permeability and fracture gas pressure. With a greater ε_{bc}^{P} value, the coal is less prone to damage.

Figure 8a shows the permeability distribution around the borehole under different equivalent plastic strains. ε_{bc}^{P} = 0 indicates that the coal is in the elastic stage, where the maximum permeability around the borehole is 1.6 k_0. This is inconsistent with the understanding that a fractured zone is formed around the borehole, resulting in a significant increase in permeability. Therefore, the elastic permeability model could not accurately reflect the borehole gas extraction process. As ε_{bc}^{P} increases, the damage zone formed around the borehole decreases, while the peak permeability of the damage zone increases. With ε_{bc}^{P} = 0.01, the permeability at the nearest point of the borehole is 12 times that of the initial value. With ε_{bc}^{P} = 0.04, the permeability is 202 k_0. In actual borehole gas extraction practices, permeability around the borehole may rise by hundreds of times. Figure 8b shows the fracture gas pressure distribution around the borehole under different equivalent plastic strains. With ε_{bc}^{P} = 0, the gas pressure increases linearly. A small, smooth, and low-pressure zone is formed around the borehole at ε_{bc}^{P} = 0.01, while the gas pressure value decreases as ε_{bc}^{P} becomes bigger, particularly in the low-pressure zone.

4.2.2. Effect of Lateral Pressure Coefficient. There are horizontal and vertical stresses around the borehole, i.e., $\boldsymbol{\sigma}_x$ and $\boldsymbol{\sigma}_y$. λ is the lateral pressure coefficient representing the ratio of horizontal stress to vertical stress. The horizontal stresses are set to be 10, 12, 14, and 16 MPa to study the effects of different lateral pressure coefficients λ (0.56, 0.67, 0.78, and 0.89) on borehole gas extraction.

It could be observed from Figure 9a that the degree of shear failure gradually decreases with the increase in the lateral pressure coefficient. As a result, the shear damage zone around

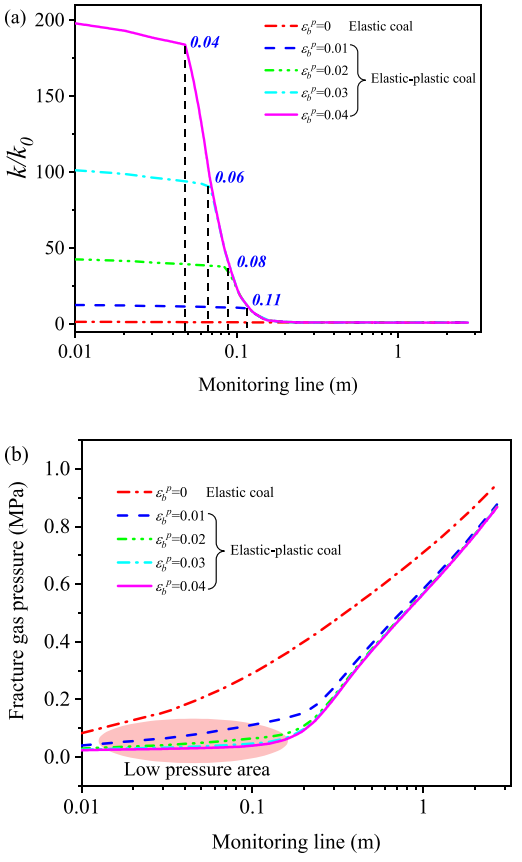

Figure 8. Effects of equivalent plastic strain on permeability and gas pressure in damaged coal. (a) Permeability; (b) fracture gas pressure.

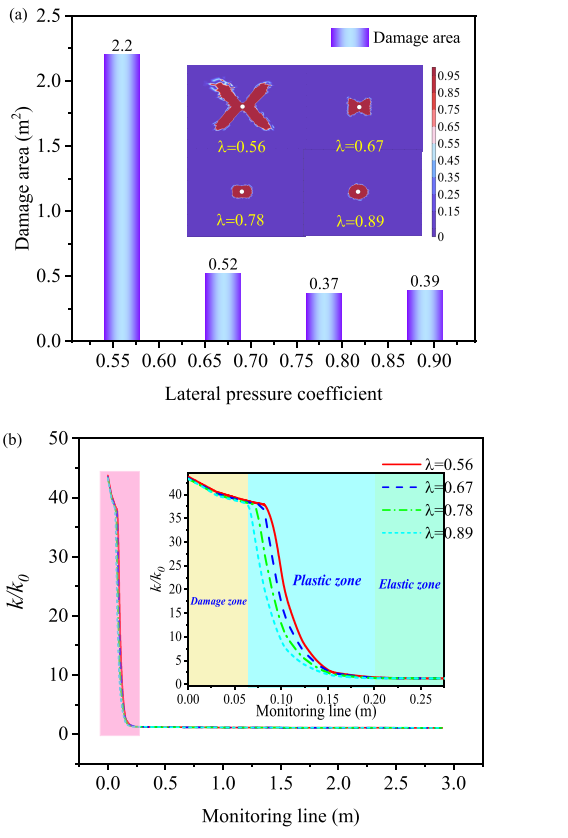

Figure 9. Damage and permeability variations around the borehole corresponding to different lateral pressure coefficients. (a) Damage zone; (b) permeability.

https://doi.org/10.1021/acsomega.4c01081
ACS Omega 2024, 9, 19578−19590

the borehole gradually decreases, while its shape gradually shifts from a butterfly distribution to a circular distribution. The area of the damage zone corresponding to the lateral pressure coefficient of 0.56 is 2.2 m^2, while that corresponding to the lateral pressure coefficient of 0.89 is 0.39 m^2, a relative reduction of 82.2%. According to Figure 9b, permeability gradually decreases as the lateral pressure coefficient increases. At the extraction time of 300 days, permeability around the borehole gradually decreases when being farther from the borehole, with permeability reaching 43 k_0 at the nearest point to the borehole. With an increasing lateral pressure coefficient, the damage and plastic zones become smaller, while elastic zone increases.

As shown in Figure 10a, fracture gas pressure varies slightly, corresponding to different lateral pressure coefficients. In the

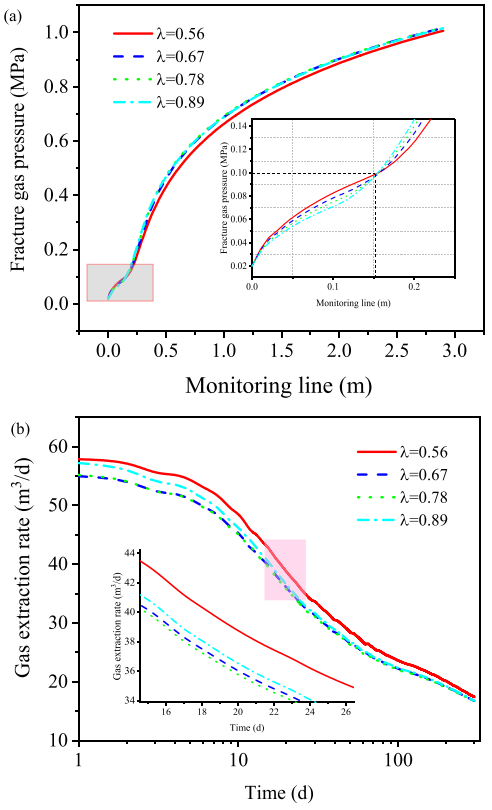

Figure 10. Borehole gas extraction performance corresponding to different lateral pressure coefficients. (a) Gas pressure; (b) borehole extraction rate

damage zone, gas pressure is smaller in cases of greater lateral pressure coefficients, but gas pressure in the plastic and elastic zones is bigger. Reason is that greater lateral pressure coefficients at closer distances to borehole could lead to more damage, increasing coal permeability and lowering gas pressure in coal. At greater distances from borehole, the lateral pressure coefficient has little effect on coal in plastic and elastic zones, resulting in decreased initial permeability and a higher gas pressure. As shown in Figure 10b, the extraction rate drops first before rising with increasing lateral pressure coefficient. At the extraction time of 10 days, the extraction rate decreases from 48 m^3/d to 45 m^3/d as the lateral pressure coefficient increases from 0.56 to 0.78. However, extraction rate shows a slightly increasing trend as lateral pressure coefficient continues to increase.

4.2.3. Effect of Internal Friction Angle. During gas extraction, the internal friction angle is a significant parameter affecting the interaction between coal particles and, thus, coal damage. Field studies show that drilling boreholes in different coal seams leads to relatively large coal damage differences. Yet, research on the effect of coal internal friction angle on permeability variation is less. In this section, effects of internal friction angles of 15°, 20°, 25°, and 30° on permeability of damaged coal are investigated.

Figure 11a shows the damage zones around the borehole regarding four internal friction angles. As the friction angle becoming bigger, damage zone gradually decreases and shifts from butterfly shape to elliptical shape. The damage zone area reduces from 2.2 to 0.079 m^2 as the friction angle rises from 15 to 30°, a reduction ratio of 96.4%. As shown in Figure 11b, permeability around the borehole gradually decreases with increasing distance from it. In the meantime, damage and plastic zones become smaller with friction angle getting bigger. Permeability could reach 43 k_0 in the case of 15°. Figure 11c shows the variation of fracture gas pressure on the monitoring line, where gas pressure at the same position is greater with rising friction angle. It could also be noted that gas pressure in damaged coal decreases with bigger friction angle. As shown in Figure 11d, the gas extraction rate gradually decreases with time. For larger internal friction angles, gas extraction rate is smaller. Taking the extraction time of 300d as an example, extraction rate corresponding to friction angle of 15° is 17 m^3/d, while extraction rate corresponding to friction angle of 30° being 14 m^3/d.

4.2.4. Effects of Cohesion. Borehole drilling induces significantly different damage in soft and hard coal seams, while cohesion is an important factor, reflecting coal strength. Impact of cohesion is similar to the internal friction angle stated above. Figure 12a shows the coal damage zones in conditions of different cohesions (2.5, 3.0, 4.0, and 5.0 MPa), in which shear failure zone around borehole decreases with bigger cohesion value and gradually shifts from butterfly distribution to elliptical distribution. Coal damage zone of cohesion of 2.5 MPa is 96.7% lower than that of 5 MPa. As shown in Figure 12b, the permeability decreases with increasing cohesion. At the same position near borehole, permeability corresponding to C_0 of 2.5 MPa, 3.0 MPa, 4.0 and 5.0 MPa is 43 k_0, 41 k_0, 40 k_0 and 39 k_0, respectively. Cohesion is closely related to coal strength; i.e., coal with greater cohesion is less prone to experience damage. The plastic and elastic zones around the borehole are larger. As shown in Figure 12c, fracture gas pressure at same position of coal is greater when cohesion increases. In Figure 12d, the borehole gas extraction rate is inversely proportional to coal cohesion. The maximum borehole extraction rates corresponding to cohesion of 2.5, 3.0, 4.0, and 5.0 MPa are 57 m^3/d, 47 m^3/d, 37 m^3/d and 31 m^3/d, respectively.

4.2.5. Effects of Elastic Modulus and Poisson's Ratio. Heterogeneity is one of coal's most common properties, which affects its seepage characteristics. Therefore, probability density equation based on Weibull distribution is adopted in this section to assign values to Young's modulus, so that heterogeneity of its distribution is as close as possible to the real case[43,44]:

$$f(E) = \frac{m}{E_0}\left(\frac{E}{E_0}\right)^{m-1} \exp\left(-\left(\frac{E}{E_0}\right)^{m}\right) \quad (23)$$

where E represents Young's modulus, E_0 denotes average Young's modulus, and m is homogeneity index defining shape of distribution function.

https://doi.org/10.1021/acsomega.4c01081
ACS Omega 2024, 9, 19578−19590

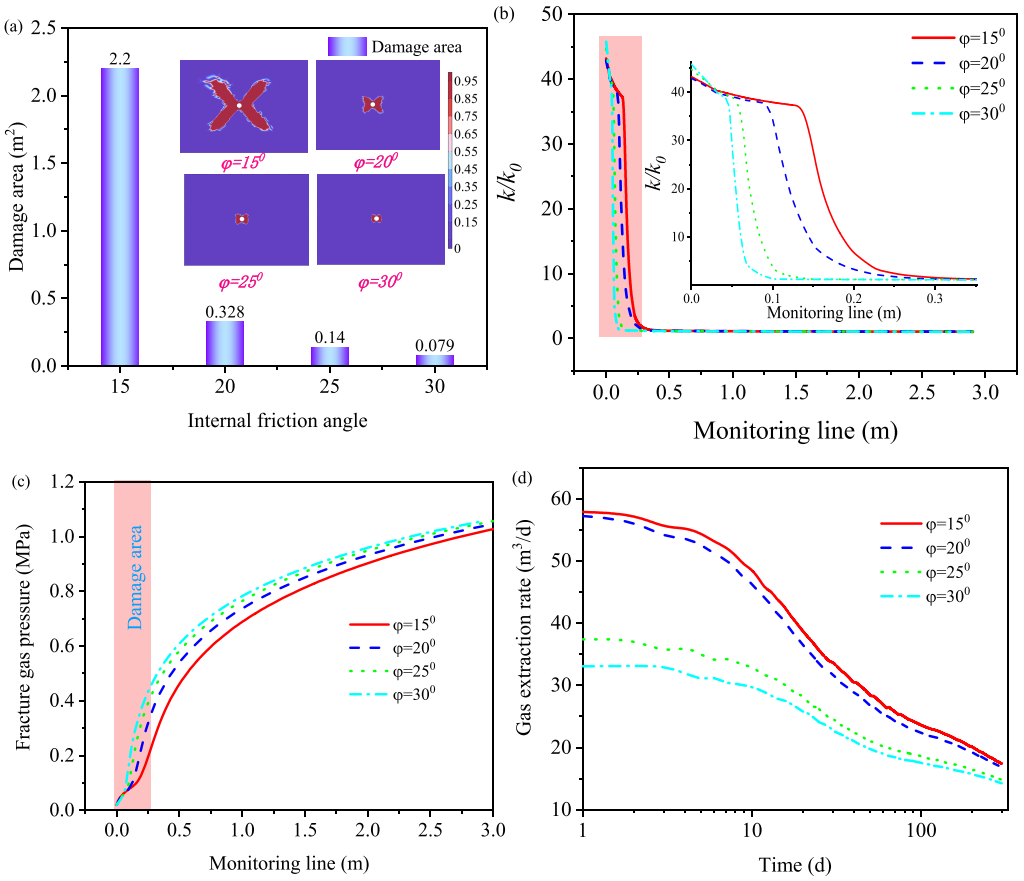

Figure 11. Borehole gas extraction performance corresponding to different internal friction angles: (a) Damage zone; (b) permeability; (c) gas pressure; (d) borehole extraction rate.

Figure 13 shows interval distribution of Young's modulus with different shape parameters of Weibull distribution. The shape parameters of 2, 4, 6, and 8 are adopted,[45] while initial Young's modulus of coal is 2500 MPa. It can be observed from Figure 13a–d that with the increase in *m*, Young's modulus values of more units approach the average Young's modulus. The average Young's moduli with m being 2, 4, 6, and 8 are 2008 MPa, 2286 MPa, 2363 and 2402 MPa, respectively. Young's modulus distribution interval corresponding to m = 2 is 1 to 7 GPa, while Young's modulus distribution interval with m = 8 is 1 to 3.3 GPa. This distribution indicates that Young's modulus distribution interval is wider with smaller homogeneity indices, while Young's modulus values are more concentrated around average value in the case of larger homogeneity indices.

Figure 14a shows that due to heterogeneous distribution of coal Young's modulus, scattered-dot damage area is observed in coal except for large shear damage area around borehole. As the homogeneity index of the Weibull distribution increases, the shear damage around the borehole and damage points far from the borehole gradually decrease. Punctate microdamage areas may gradually expand during gas drainage, leading to better fracture development within coal. As a result, the permeability increases, which is beneficial to long-term gas extraction efficiency. However, those microdamaged areas may also become gas-accumulation areas, thereby good gas drainage should be conducted in these areas.

In terms of the effect of Poisson's ratio, the damage zone continuously drops as Poisson's ratio rises from 0.25 to 0.40. This is because Poisson's ratio is the ratio of lateral strain to longitudinal strain. Larger Poisson ratios indicate that energy tends to be continuously transferred rather than accumulated under greater transverse strains under the same conditions. Figure 14b shows that as Poisson's ratio rises, the resulting maximum permeability gradually reduces. At the same position in coal, permeability corresponding to Poisson's ratios of 0.25, 0.30, 0.35, and 0.40 are 44.7 k_0, 43.9 k_0, 43.2 k_0 and 42.5 k_0, respectively. Figure 14c shows that fracture gas pressure near the borehole is basically the same for different Poisson's ratios. Meanwhile, the gas pressure is greater at positions farther away from borehole, which grows with the increase of Poisson's ratio. As shown in Figure 14d, gas extraction rates regarding four Poisson's ratios drop rapidly first and then slowly with the extraction time. Meanwhile, the gas extraction rate is lower with larger initial Poisson's ratios. At the initial stage of extraction, extraction rates are 51 m^3/d, 47 m^3/d, 45 m^3/d and 44 m^3/d when Poisson's ratios being 0.25, 0.30, 0.35 and 0.40.

5. CONCLUSIONS

(1) A fluid–solid coupling model taking into account coal stress, gas seepage, gas diffusion, and coal damage is established for more accurately analyzing damage properties around borehole and gas flow characteristics. Coal damage degree is quantified with equivalent plastic strain ε_{bc}^{p}. Permeability of the damaged coal increases sharply. Thus, neglecting the impact of damage on permeability could cause gas production underestimation. Damage-based permeability shows a three-zone distribution around borehole, i.e. permeability is the highest in the

https://doi.org/10.1021/acsomega.4c01081
ACS Omega 2024, 9, 19578–19590

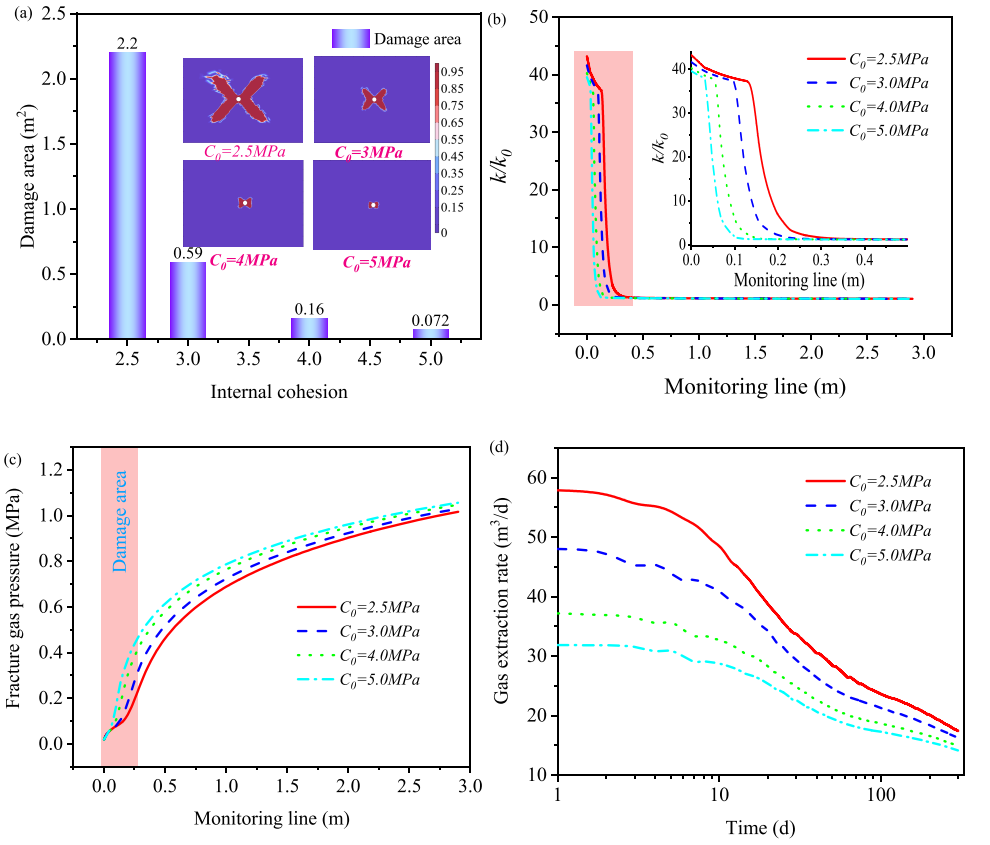

Figure 12. Borehole gas drainage parameter variations regarding four cohesion values. (a) Damage zone; (b) permeability; (c) gas pressure; (d) borehole extraction rate.

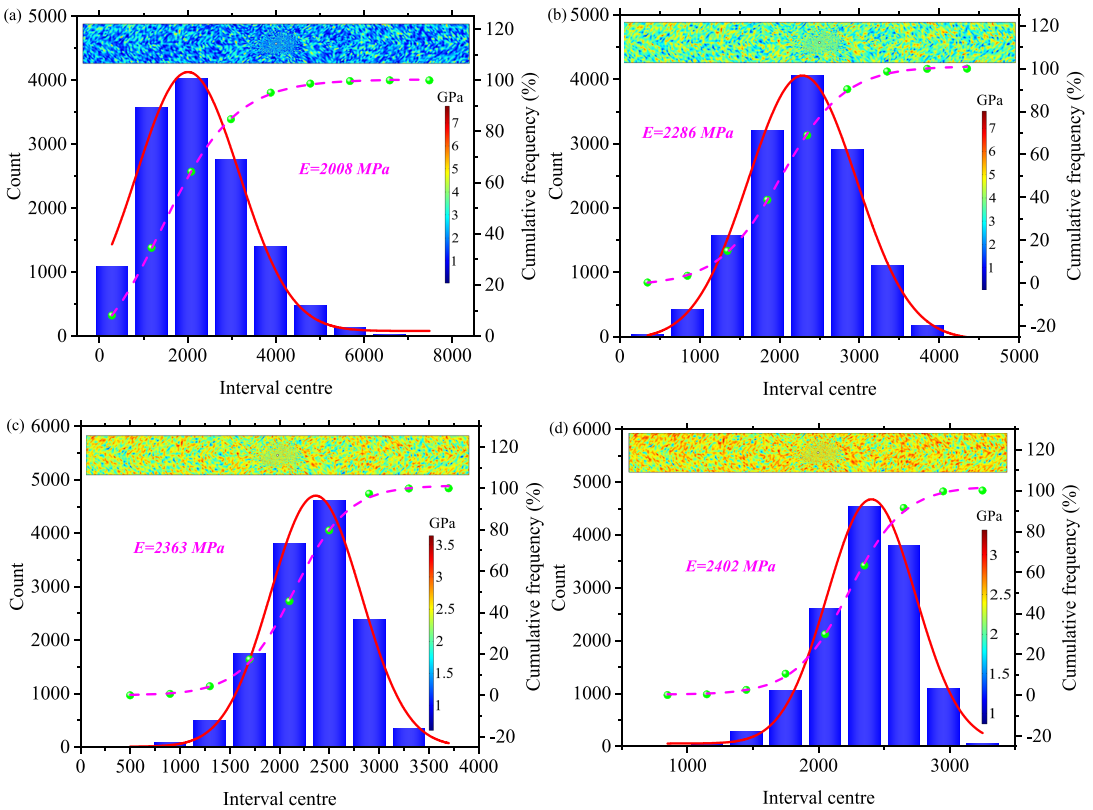

Figure 13. Young's modulus distribution intervals corresponding to different shape parameters of Weibull distribution. (a) $m = 2$; (b) $m = 4$; (c) $m = 6$; (d) $m = 8$.

https://doi.org/10.1021/acsomega.4c01081
ACS Omega 2024, 9, 19578−19590

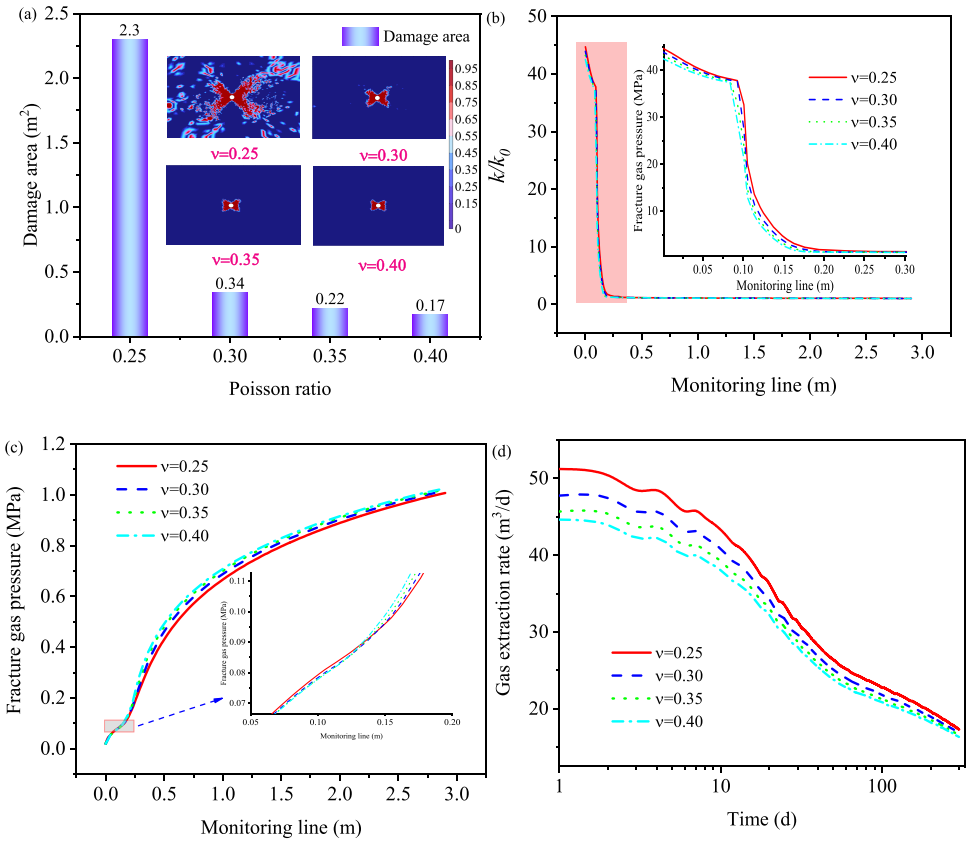

Figure 14. Borehole gas extraction performance corresponding to four Poisson's ratios. (a) Damage zone; (b) permeability; (c) gas pressure; (d) borehole extraction rate.

fracture zone, approximately 40 times the original permeability; Permeability of the plastic zone decreases rapidly, while the permeability of the elastic zone is close to the original value. In the gas extraction process, coal permeability in the damage zone rises rapidly, in which fracture and matrix gas pressure change show a smooth low-value zone.

(2) As the equivalent plastic strain rises, the damage zone around the borehole decreases, while the peak permeability in the damage zone keeps rising. Gas pressure smooth low-pressure zone around the borehole drops. Increasing lateral pressure coefficient causes the shear damage zone around the borehole to reduce gradually, with the damage zone shifting from a butterfly shaped distribution to a circular distribution. However, plastic and elastic zones increase. When the lateral pressure coefficient increases from 0.56 to 0.89, the damage area relatively reduces by 82.3%. As internal friction angle and cohesion increase, the damage zone around the borehole decreases and shifts from butterfly shape to elliptical shape.

(3) When Young's modulus of coal is heterogeneously distributed, except for concentrated shear damage zones around borehole, scattered-dot damage zones also occur in coal area with low strength. As the homogeneity index of Weibull distribution becomes larger, the shear damage zones around borehole and scattered-dot damage zones away from borehole gradually decrease. Meanwhile, when Poisson's ratio increases from 0.25 to 0.40, the area of damage zone decreases. In future studies, effects of borehole air leakage and coal seam temperature on the gas extraction process are expected to be further included to obtain more accurate results.

AUTHOR INFORMATION

Corresponding Authors

Chunshan Zheng − *Joint National-Local Engineering Research Centre for Safe and Precise Coal Mining and School of Safety Science and Engineering, Anhui University of Science and Technology, Huainan 232001, China;* orcid.org/0000-0003-0255-6005; Email: chunshanzheng@aust.edu.cn

Guofu Li − *State Key Laboratory of Coal and Coalbed Methane Co-Mining, Jincheng 048012, China*; Email: Futn999@126.com

Authors

Haifei Wu − *Joint National-Local Engineering Research Centre for Safe and Precise Coal Mining and School of Safety Science and Engineering, Anhui University of Science and Technology, Huainan 232001, China*

Sheng Xue − *Joint National-Local Engineering Research Centre for Safe and Precise Coal Mining and School of Safety Science and Engineering, Anhui University of Science and Technology, Huainan 232001, China*

Bingyou Jiang − *Joint National-Local Engineering Research Centre for Safe and Precise Coal Mining and School of Safety Science and Engineering, Anhui University of Science and Technology, Huainan 232001, China;* orcid.org/0000-0002-2751-7347

Mingyun Tang − *School of Safety Science and Engineering, Anhui University of Science and Technology, Huainan 232001, China*

https://doi.org/10.1021/acsomega.4c01081
ACS Omega 2024, 9, 19578−19590

Complete contact information is available at:
https://pubs.acs.org/10.1021/acsomega.4c01081

Notes

The authors declare no competing financial interest.

■ ACKNOWLEDGMENTS

This work is financially supported by National Natural Science Foundation of China (52274171), Excellent Youth Project of Universities in Anhui Province (2023AH030042), Joint National-Local Engineering Research Centre for Safe and Precise Coal Mining Fund (EC2023015), Unveiled List of Bidding Projects of Shanxi Province (20201101001).

■ REFERENCES

(1) Kong, X.; Wang, E.; Liu, X.; Li, N.; Chen, L.; Feng, J.; Kong, B.; Li, D.; Liu, Q. Coupled analysis about multi-factors to the effective influence radius of hydraulic flushing: Application of response surface methodology. *Journal of Natural Gas Science and Engineering* **2016**, *32*, 538−548.

(2) Li, S.; Fan, C.; Han, J.; Luo, M.; Yang, Z.; Bi, H. A fully coupled thermal-hydraulic-mechanical model with two-phase flow for coalbed methane extraction. *Journal of Natural Gas Science and Engineering* **2016**, *33*, 324−336.

(3) Zhao, Y.; Lin, B.; Liu, T.; Li, Q.; Kong, J. Gas flow field evolution around hydraulic slotted borehole in anisotropic coal. *Journal of Natural Gas Science and Engineering* **2018**, *58*, 189−200.

(4) Fan, C.; Elsworth, D.; Li, S.; Chen, Z.; Luo, M.; Song, Y.; Zhang, H. Modelling and optimization of enhanced coalbed methane recovery using CO2/N-2 mixtures. *Fuel* **2019**, *253*, 1114−1129.

(5) Lin, B.; Song, H.; Zhao, Y.; Liu, T.; Kong, J.; Huang, Z. Significance of gas flow in anisotropic coal seams to underground gas drainage. *J. Pet. Sci. Eng.* **2019**, *180*, 808−819.

(6) Zhao, Y.; Lin, B.; Liu, T.; Kong, J.; Zheng, Y. Gas flow in hydraulic slotting-disturbed coal seam considering stress relief induced damage. *J. Nat. Gas Sci. Eng.* **2020**, *75*, No. 103160.

(7) Bai-quan, L.; Ting, L.; Quan-le, Z.; Chuan-jie, Z.; Fa-zhi, Y.; Zhen, Z. Crack propagation patterns and energy evolution rules of coal within slotting disturbed zone under various lateral pressure coefficients. *Arab. J. Geosci.* **2015**, *8* (9), 6643−6654.

(8) Liu, T.; Lin, B.; Fu, X.; Zhu, C. Modeling air leakage around gas extraction boreholes in mining-disturbed coal seams. *Process Safety and Environmental Protection* **2020**, *141*, 202−214.

(9) Li, H.; Li, X.; Fu, J.; Zhu, N.; Chen, D.; Wang, Y.; Ding, S.Experimental study on compressive behavior and failure characteristics of imitation steel fiber concrete under uniaxial load. *Construction and Building Materials***2023**, *399*, 132599.

(10) Zheng, C.; Li, H.; Kizil, M.; Jiang, B.; Xue, S.; Yang, W.; Chen, Z.Performance enhancement of horizontal underground-to-inseam gas drainage boreholes with double-phase-grouting sealing method for coal mining safety and clean gas resource. *Journal of Natural Gas Science and Engineering***2020**, *76*, 103179.

(11) Fan, D.; Ettehadtavakkol, A. Analytical model of gas transport in heterogeneous hydraulically-fractured organic-rich shale media. *Fuel* **2017**, *207*, 625−640.

(12) Zhang, C.; Xu, J.; Peng, S.; Li, Q.; Yan, F. Experimental study of drainage radius considering borehole interaction based on 3D monitoring of gas pressure in coal. *Fuel* **2019**, *239*, 955−963.

(13) Zhang, R.; Cheng, Y.; Yuan, L. Study on the stress relief and permeability increase in a special low-permeability thick coal seam to stimulate gas drainage. *Energy Sources Part a-Recovery Utilization and Environmental Effects* **2020**, *42* (8), 1001−1013.

(14) Cao, P.; Liu, J.; Leong, Y.-K. A multiscale-multiphase simulation model for the evaluation of shale gas recovery coupled the effect of water flowback. *Fuel* **2017**, *199*, 191−205.

(15) Chen, D.; Pan, Z.; Liu, J.; Connell, L. D. Characteristic of anisotropic coal permeability and its impact on optimal design of multi-lateral well for coalbed methane production. *J. Pet. Sci. Eng.* **2012**, *88*, 13−28.

(16) Duan, M.; Jiang, C.; Gan, Q.; Zhao, H.; Yang, Y.; Li, Z. Study on permeability anisotropy of bedded coal under true triaxial stress and its application. *Transport in Porous Media* **2020**, *131* (3), 1007−1035.

(17) Fang, H.-H.; Zheng, C.-S.; Qi, N.; Xu, H.-J.; Liu, H.-H.; Huang, Y.-H.; Wei, Q.; Hou, X.-W.; Li, L.; Song, S.-L. Coupling mechanism of THM fields and SLG phases during the gas extraction process and its application in numerical analysis of gas occurrence regularity and effective extraction radius. *Petroleum Science* **2022**, *19* (3), 990−1006.

(18) Liu, T.; Lin, B.; Yang, W.; Liu, T.; Kong, J.; Huang, Z.; Wang, R.; Zhao, Y. Dynamic diffusion-based multifield coupling model for gas drainage. *Journal of Natural Gas Science and Engineering* **2017**, *44*, 233−249.

(19) Zheng, C.; Kizil, M. S.; Chen, Z.; Aminossadati, S. M. Role of multi-seam interaction on gas drainage engineering design for mining safety and environmental benefits: Linking coal damage to permeability variation. *Process Safety and Environmental Protection* **2018**, *114*, 310−322.

(20) Qi, E.; Xiong, F.; Cao, Z.; Zhang, Y.; Xue, Y.; Zhang, Z.; Ji, M. Simulation of Gas Fracturing in Reservoirs Based on a Coupled Thermo-Hydro-Mechanical-Damage Model. *Applied Sciences* **2024**, *14* (5), 1763.

(21) Liu, H.; Li, X.; Yu, Z.; Tan, Y.; Ding, Y.; Chen, D.; Wang, T. Influence of hole diameter on mechanical properties and stability of granite rock surrounding tunnels. *Phys. Fluids* **2023**, *35* (6), No. 064121.

(22) Zheng, C.; Jiang, B.; Xue, S.; Chen, Z.; Li, H. Coalbed methane emissions and drainage methods in underground mining for mining safety and environmental benefits: A review. *Process Safety and Environmental Protection* **2019**, *127*, 103−124.

(23) Wang, C.; Zhao, Y.; Ning, L.; Bi, J. Permeability evolution of coal subjected to triaxial compression based on in-situ nuclear magnetic resonance. *International Journal of Rock Mechanics and Mining Sciences* **2022**, *159*, No. 105213.

(24) Fan, C.; Elsworth, D.; Li, S.; Zhou, L.; Yang, Z.; Song, Y. Thermo-hydro-mechanical-chemical couplings controlling CH4 production and CO2 sequestration in enhanced coalbed methane recovery. *Energy* **2019**, *173*, 1054−1077.

(25) Nian, F.; Ju, F.; Zheng, C.; Wu, H.; Cheng, X.Effects of Coal Permeability Anisotropy on Gas Extraction Performance. *Processes***2023**, *11* (5), 1408.

(26) Si, L.; Li, Z.; Yang, Y.; Gao, R. The stage evolution characteristics of gas transport during mine gas extraction: Its application in borehole layout for improving gas production. *Fuel* **2019**, *241*, 164−175.

(27) Liu, Q.; Cheng, Y.; Zhou, H.; Guo, P.; An, F.; Chen, H. A mathematical model of coupled gas flow and coal deformation with gas diffusion and Klinkenberg effects. *Rock Mechanics and Rock Engineering* **2015**, *48* (3), 1163−1180.

(28) Li, W.; Liu, J.; Zeng, J.; Leong, Y.-K.; Elsworth, D.; Tian, J.; Li, L. A fully coupled multidomain and multiphysics model for evaluation of shale gas extraction. *Fuel* **2020**, *278*, No. 118214.

(29) Zhu, W. C.; Wei, C. H.; Liu, J.; Qu, H. Y.; Elsworth, D. A model of coal−gas interaction under variable temperatures. *International Journal of Coal Geology* **2011**, *86* (2−3), 213−221.

(30) Wu, Y.; Liu, J.; Elsworth, D.; Siriwardane, H.; Miao, X. Evolution of coal permeability: Contribution of heterogeneous swelling processes. *International Journal of Coal Geology* **2011**, *88* (2−3), 152−162.

(31) An, F.; Cheng, Y.; Wang, L.; Li, W. A numerical model for outburst including the effect of adsorbed gas on coal deformation and mechanical properties. *Computers and Geotechnics* **2013**, *54*, 222−231.

(32) Fan, Z.; Zhang, D.; Fan, G.; Zhang, L.; Zhang, S.; Liang, S.; Yu, W.; Gao, S.; Guo, W. Non-Darcy thermal-hydraulic-mechanical damage model for enhancing coalbed methane extraction. *Journal of Natural Gas Science and Engineering***2021**, *93*, DOI: 10.1016/j.jngse.2021.104048.

(33) Liu, Q.; Cheng, Y.; Haifeng, W.; Hongxing, Z.; Liang, W.; Wei, L.; Hongyong, L. Numerical assessment of the effect of equilibration

time on coal permeability evolution characteristics. *Fuel* **2015**, *140*, 81−89.
(34) Zhao, Y.; Lin, B.; Liu, T.; Zheng, Y.; Kong, J.; Li, Q.; Song, H.Mechanism of multifield coupling-induced outburst in mining-disturbed coal seam. *Fuel***2020**, *272*, 117716.
(35) Zhao, Y.; Lin, B.; Liu, T.Thermo-hydro-mechanical couplings controlling gas migration in heterogeneous and elastically-deformed coal. *Computers and Geotechnics***2020**, *123*, 103570.
(36) Yang, L.; Fan, C.; Wen, H.; Luo, M.; Sun, H.; Jia, C.An improved gas-liquid-solid coupling model with plastic failure for hydraulic flushing in gassy coal seam and application in borehole arrangement. *Phys. Fluids* **2023**, *35* (3), .
(37) Liu, T.; Lin, B.; Fu, X.; Zhao, Y.; Gao, Y.; Yang, W. Modeling coupled gas flow and geomechanics process in stimulated coal seam by hydraulic flushing. *International Journal of Rock Mechanics and Mining Sciences* **2021**, *142*, No. 104769.
(38) Zheng, C.; Wu, H.; Jiang, B.; Xue, S.; Zhao, Y. Investigation on interaction effects of multiple factors on clean gas extraction: implementation of response surface methodology. *Journal of Geophysics and Engineering* **2023**, *20* (6), 1095−1108.
(39) Gao, F.; Xue, Y.; Gao, Y.; Zhang, Z.; Teng, T.; Liang, X. Fully coupled thermo-hydro-mechanical model for extraction of coal seam gas with slotted boreholes. *Journal of Natural Gas Science and Engineering* **2016**, *31*, 226−235.
(40) Su, E.; Liang, Y.; Zou, Q.; Xu, M.; Sasmito, A. P. Numerical analysis of permeability rebound and recovery during coalbed methane extraction: Implications for CO2 injection methods. *Process Safety and Environmental Protection* **2021**, *149*, 93−104.
(41) Zhang, H.; Cheng, Y.; Liu, Q.; Yuan, L.; Dong, J.; Wang, L.; Qi, Y.; Wang, W. A. novel in-seam borehole hydraulic flushing gas extraction technology in the heading face: Enhanced permeability mechanism, gas flow characteristics, and application. *Journal of Natural Gas Science and Engineering* **2017**, *46*, 498−514.
(42) Zhang, H.; Cheng, Y.; Deng, C.; Shu, L.; Pan, Z.; Yuan, L.; Wang, L.; Liu, Q. A. Novel In-Seam Borehole Discontinuous Hydraulic Flushing Technology in the Driving Face of Soft Coal Seams: Enhanced Gas Extraction Mechanism and Field Application. *Rock Mechanics and Rock Engineering* **2022**, *55* (2), 885−907.
(43) Zhu, W. C.; Wei, C. H. Numerical simulation on mining-induced water inrushes related to geologic structures using a damage-based hydromechanical model. *Environmental Earth Sciences* **2011**, *62* (1), 43−54.
(44) Zheng, C.; Kizil, M. S.; Aminossadati, S. M.; Chen, Z. Effects of geomechanical properties of interburden on the damage-based permeability variation in the underlying coal seam. *Journal of Natural Gas Science and Engineering* **2018**, *55*, 42−51.
(45) Zheng, C.; Jiang, B.; Yuan, L.; Kizil, M.; Xue, S.; Han, B.; Tang, M.; Chen, Z. Effects of heterogenous interburden Young's modulus on permeability characteristics of underlying relieved coal seam: Implementation of damage-based permeability model. *Journal of Natural Gas Science and Engineering* **2021**, *96*, No. 104317.

https://doi.org/10.1021/acsomega.4c01081
ACS Omega 2024, 9, 19578−19590